공학석사 학위논문

Development of New Concept of Wind Tunnel Test: Real-Time Aeroelastic Hybrid Simulation

신개념 풍동실험 장비의 개발: 실시간 공탄성 하이브리드 시뮬레이션

2021 년 2 월

서울대학교 대학원

건설환경공학부

심 재 홍

Development of New Concept of Wind Tunnel Test: Real-Time Aeroelastic Hybrid Simulation

신개념 풍동실험 장비의 개발: 실시간 공탄성 하이브리드 시뮬레이션

지도교수 김 호 경

이 논문을 공학석사 학위논문으로 제출함

2021년 2월

서울대학교 대학원

건설환경공학부

심 재 홍

심재홍의 공학석사 학위논문을 인준함

2020년 12월

위 원 장 _____ 이 해 성 _____ (인)

부위원장 _____ 김 호 경 _____ (인)

위 원 _____ 송 준 호 _____ (인)

ABSTRACT

Development of New Concept of Wind Tunnel Test: Real-Time Aeroelastic Hybrid Simulation

Jae Hong Shim
Department of Civil and Environmental Engineering
Seoul National University

This study proposes a new concept for wind tunnel tests of bridges and aims to develop equipment and review the applicability to wind tunnel tests using the proposed method. The proposed new wind tunnel test method is performed through interaction between the two by applying real-time hybrid techniques to wind tunnel experiments and dividing wind tunnel experiments into experimental and numerical systems.

The real-time aeroelastic hybrid simulation(RTAHS) system measures wind-induced forces through actual experiments and, in the cyber system, calculates the bridge deck's displacement in real-time. This RTAHS system accurately measures wind-induced forces, which were difficult to measure in conventional wind tunnel tests. And the dynamic characteristics of the system were implemented more efficiently and more accurately numerically.

The RTAHS system consists of hardware and software components. A hardware system comprises four linear motors, the controller to control them,

load cell, and accelerometer. The software system includes a numerical integration program for the calculation of the equation of motion, a time delay compensation program, and a PI control program for precise control.

The verification of the RTAHS system's software component is performed. The removal of inertial force due to the mass of the bridge deck model and the compensation of the time delay of 18 ms of the system are properly performed through the real-time calculation of the equation of motion and the Improved AIC method.

The RTAHS system's applicability to wind tunnel test was confirmed through free vibration tests with the force feedback process and vibration tests to observe the bridge deck's vortex-induced vibration in the wind tunnel. The difference between the system's apparent damping ratio and the target value is the effect of the residual time delay after delay compensation. Through a comparative experiment using the developed and conventional system with a rectangular section of B/D = 5, the vortex-induced vibration was observed at the same wind speed range, and the results of displacement were also confirmed to be reasonable. Therefore, the proposed RTAHS system can well simulate two-dimensional wind tunnel tests within the identified range.

Keywords: Wind tunnel test; Real-time aeroelastic hybrid simulation; Time-delay compensation; Bridge deck; Linear motor;

Student Number: 2019-26624

TABLE OF CONTENTS

LIST OF FIGURES

LIST OF TABLES

CHAPTER 1

INTRODUCTION

1.1 Research Background

With the development of technology, long-span and light-weighted bridges have been constructed. As the span of a bridge gets longer, the natural frequency and damping ratio decrease, which makes the bridge sensitive to wind-induced vibration. The vortex-induced vibration that excites the bridge with the vortex shedding caused by separated wind and the flutter, dynamic instability of an elastic structure in a fluid flow, caused by positive feedback between the body's deflection and the force exerted by the fluid flow are the representative examples of such things.

For a long-span cable-supported bridge, the bridge deck's aerodynamic properties are the main parameters affecting the vibration and stability of a bridge by wind loads. Therefore, it is required to consider the wind effect on the long-span cable-supported bridge. To evaluate the stability of a bridge under the wind , wind tunnel tests are widely used.

The 2D section model wind tunnel test is an experiment in which representative sections of structures with two-dimensional characteristics such as reinforcement girders, cables, and chimneys are made into rigid models. Sectional model tests include vibration tests conducted by spring support systems. Several dynamic characteristics, such as stiffness, mass, and damping, are to

be scaled with similitude laws to assess the wind-induced vibration by vibration test shown in Figure 1.1. Added mass, oil damper, and spring are used to simulates inertia, damping, and stiffness in the modal space.

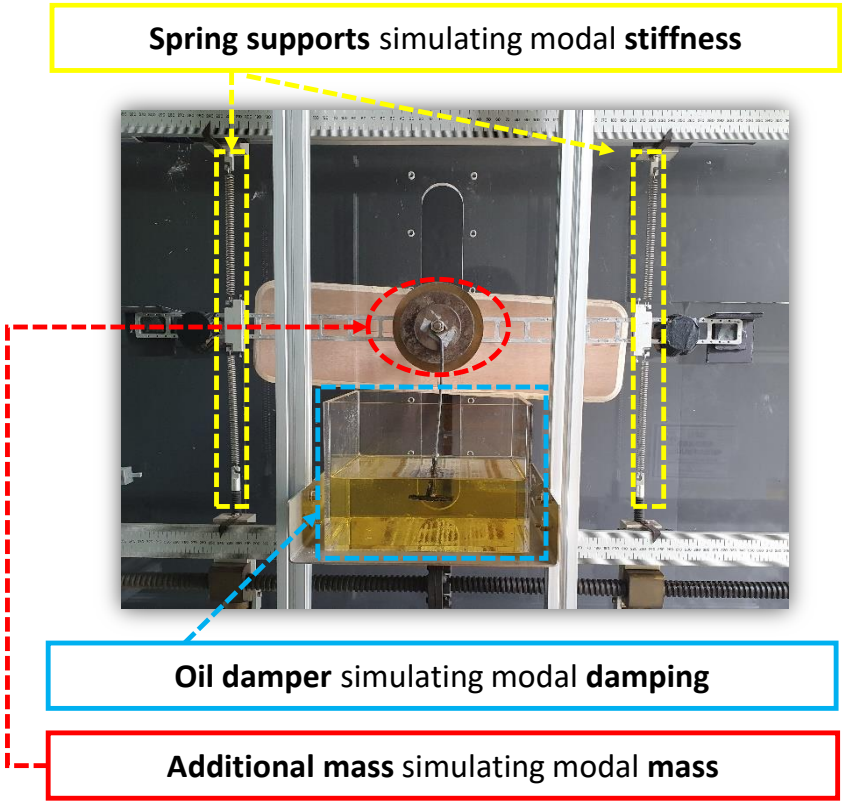

Figure 1.1 Spring support wind tunnel test

1.2 New Concept for the Wind Tunnel Test

Structural systems have traditionally been explored using experimental methods or analytical models. In general, full-scale testing is the most realistic method for evaluating structural systems. However, this usually requires equipment that is not readily available in the laboratory, and also an equipment capacity is a problem. On the other hand, analytical models are limited to solving certain types of problems, and in many cases, fail to capture complex behavior or failure modes at the structural system level. While combining both experimental and analytical tools in a single simulation, what each tool provides is called hybrid simulation.

In hybrid simulations, the structure can be divided into experimental or numerical substructures or various components consisting of a combination of the two. This simulation technique makes it possibles to represent the entire structural system by utilizing various models on various elements. In general, well-understood components are computationally modeled as numerical substructures, while difficult-to-model components are physically tested as experimental substructures. Therefore, hybrid simulations provide an efficient and cost-effective approach for the evaluation of structural systems.

In real-time hybrid simulation (RTHS) tests (e.g., seismic applications), the main advantage is that the entire system can be divided into experimental(physical) and computational(cyber) substructures, and the interaction between them is implemented via a shaking table and dynamic actuator (Shao

et al. 2010). However, the RTHS concept may not be directly applicable in wind engineering applications, so a limited RTHS application has been developed to advance the simulation of wind effects on structures. Kanda et al. (2003), Kato and Kanda (2014) developed a hybrid testing technique for simulating buildings' reactions under wind forces. Wu et al. (2019) proposed a real-time aerodynamics hybrid simulation of section model test considering interactions between the actuators and building models. However, the verification and validation by the real test were not discussed in their study.

In real-time tests, the delay in the actuator's response is the main issue for system stability. To solve this time-delay problem, Chen and Ricles (2009) proposed the inverse compensation method using a simplified first-order discrete transfer function for servo-hydraulic response under actuator. Chen and Ricles (2010) suggest adaptive control law for compensation using an error tracking indicator for the variable time delay. Chen et al. (2012) proposed the implemented compensation method considering the amplitude error.

1.3 Structure of the Thesis

This paper consists of five chapters to introduce each part of the proposed methodology.

This chapter describes the background of this work and a brief introduction to the proposed method. Several related works of literature are also reviewed.

Next, Chapter 2 introduces a brief description of the proposed real-time aeroelastic hybrid simulation (RTAHS) system and the system's hardware and software parts. The numerical integration method for calculating the displacement of the next step, along with the method for measuring only the net wind-induced force, is described. It includes a method for identifying the current system's time-delay characteristics and strategies to compensate for them.

Chapter 3 carries out a verification of software built for control. Apply the time-delay compensation method to verify that it compensates properly. The verification of calculation of the target displacement in real time and apply the time delay compensation method to verify that the motor has actually reached the desired position at the desired time. It also measures wind-induced forces, a major component of wind tunnel experiments, to perform comparisons with existing experiments. This provides a review of the verification of the current system.

Chapter 4 introduces the validation test the applicability of the RTAHS system to wind tunnel experiments. The validation test is performed with conditions without wind force and with wind force. Finally, Chapter 5 summarizes the main findings and contributions of this study and discusses several additional research topics.

CHAPTER 2

DEVELOPMENT OF THE RTAHS SYSTEM IN WIND TUNNEL

2.1 Proposed RTAHS Concept in the Wind Tunnel Test

The new concept of wind tunnel test with hybrid simulation technique is shown in Figure 2.1. Unlike the conventional 2D section model wind tunnel test, which measured displacement only, the new method measures wind-induced forces in an actual wind tunnel test through four load cells attached to each side of a two-dimensional deck section model. Futek's 2-axis load cell, MBA400(Figure 2.2), is used according to a previous study(Hwang, 2019), and the capacity is ±200 lb.

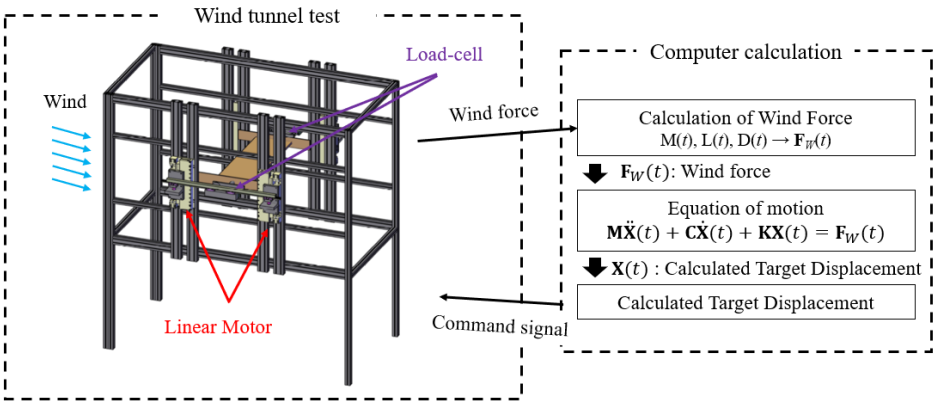

Figure 2.1 Proposed RTAHS concept in the wind tunnel test

Figure 2.2 Load cell for force measurement(Futek, MBA 400)

Measure force is used to calculate the target position in a virtual system through a basic equation of motion, along with numerically inputted dynamic properties. It reduces the time and effort used to set these dynamic characteristics in conventional wind tunnel test physically. When the next target displacement is calculated, the linear motor moves to the corresponding position and applies the movement to the model.

Four linear motors were used to enable movement of the two degrees of freedom of vertical and torsional, as conventional wind tunnel test does. Linear motors are installed on each side of the model to simulate vertical motion when moving in the same direction and simulate the torsional motion when moving in different directions, as shown in Figure 2.3. The linear motor can move with a vertical amplitude of 40 mm, and the entire system is installed in the wind tunnel, as shown in Figure 2.4.

(a) (b)

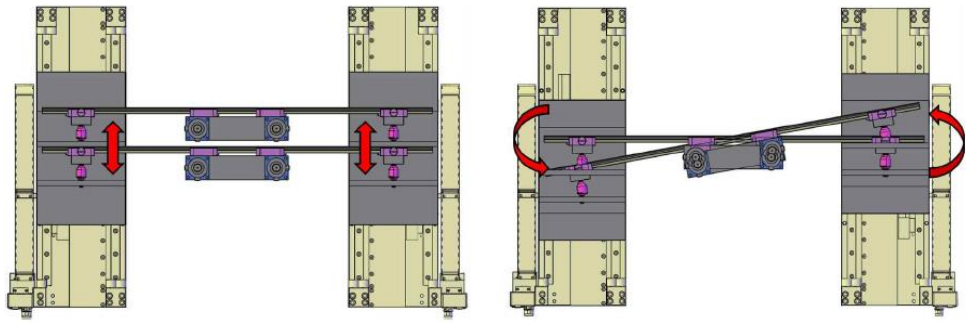

Figure 2.3 Simulate the 2DOF motion in the RTAHS system
(a) Vertical direction (b) Torsional direction

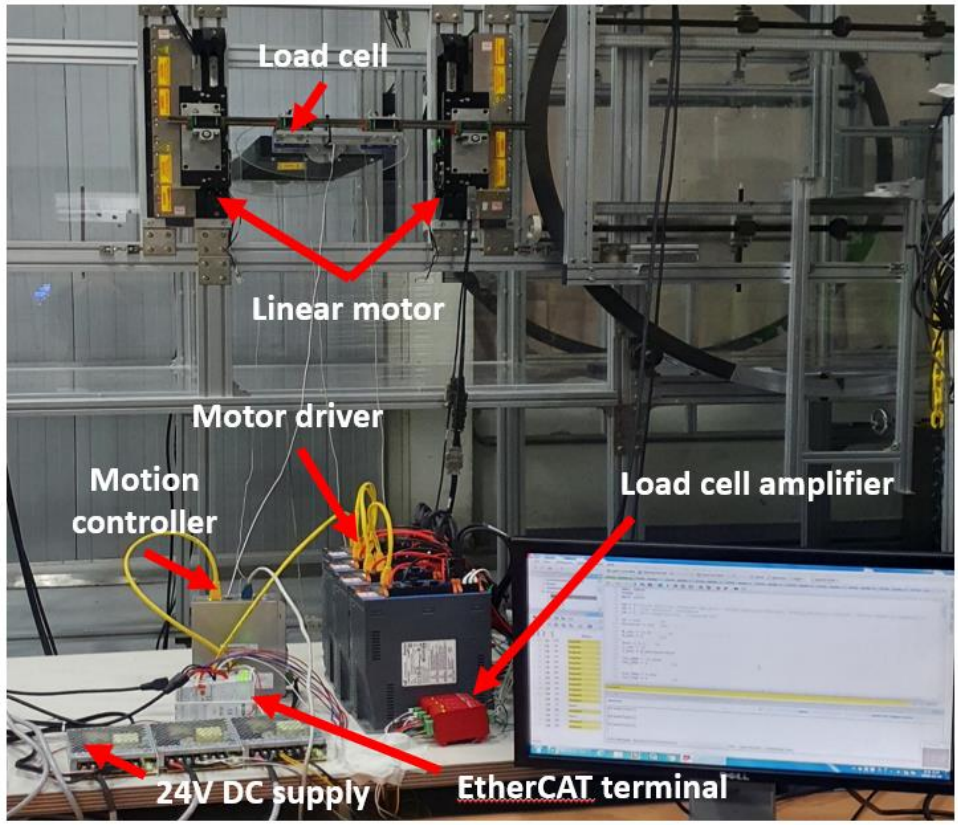

Figure 2.4 Hardware setup for RTAHS in the wind tunnel

2.2 Development of the Control System of the RTAHS System

2.2.1 The Schematic of the Control System

The RTAHS system application requires the development of the control system as well as the hardware part. The control system of the RTAHS system is performed with three loops as shown in Figure 2.5: (1) numerical integration loop, (2) time-delay compensation loop, and (3) PI control loop.

The numerical integration loop calculates the next step's target displacement($\mathbf{X}_t^{i+1}$) using the measured force and the current step's measured displacement($\mathbf{X}_m^i$) through the basic equation of motion. The time-delay compensation loop compensates for the delay and amplitude difference between the measured displacement and the target displacement. It then sends a compensated command signal($\mathbf{X}_c^{i+1}$) to the motor driver. The motor driver transmits the received signal to the motor, which operates along with the signal. The motor driver continuously calculates the difference between the desired target signal and the measured one. It is then calibrated using the proportional and integral terms of this difference through the proportional-integral(PI) control. For control systems, to reduce the instability problem observed in the previous studies (Hwang, 2019; Moni et al., 2020), ACS's SPiiPlusEC motion controller and EtherCAT connection were used to enable data communication at intervals of 2 ms.

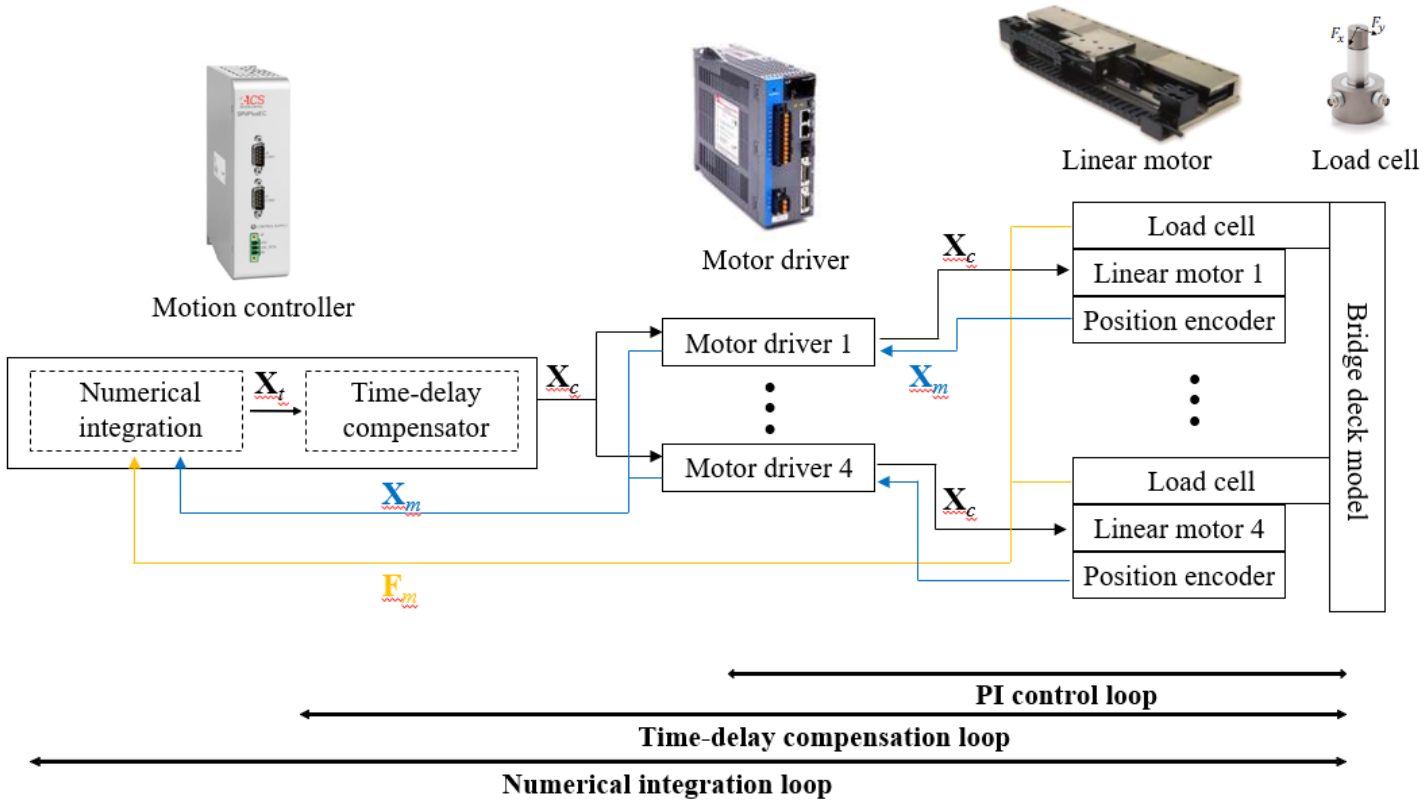

Figure 2.5 The schematic of the control system

2.2.2 Numerical Integration Scheme

A numerical integration scheme is required to calculate the next displacement in real-time. Calculate the next step's displacement by solving the governing equation from the numerical integration scheme using the current position and measured force. For this, the establishment of the governing equation is needed. The ideal governing equation under wind loads is the simple equation of motion, as shown in Equation (2.1).

$$\mathbf{M}\ddot{\mathbf{X}} + \mathbf{C}\dot{\mathbf{X}} + \mathbf{K}\mathbf{X} = \mathbf{F}_W \tag{2.1}$$

Where $\mathbf{M}$, $\mathbf{C}$, and $\mathbf{K}$ represent the target mass, damping and stiffness matrixes of the virtual system respectively, $\mathbf{X}$, $\dot{\mathbf{X}}$ and $\ddot{\mathbf{X}}$ represent the displacement, velocity, and acceleration of the physical system, respectively, $\mathbf{F}_W$ is wind-induced force.

The wind-induced force is measured by the load cell, which simultaneously measures the inertial force as well as the wind-induced force. Therefore, the process of removing the inertial force from the measured one is necessary. The inertial force can be eliminated using the specimen's acceleration measured by the accelerometer and experimental mass, as shown in Equation (2.2).

$$\mathbf{F}_W = \mathbf{F}_M + \mathbf{M}_E \ddot{\mathbf{X}}_M \tag{2.2}$$

Where $\mathbf{F}_M$ represent the measured force, $\mathbf{M}_E$ represent the experimental mass and $\ddot{\mathbf{X}}_M$ represent the measured acceleration.

To remove the inertial force using the accelerometer, the accelerometer is attached to the center of load cells shown in Figure 2.6. Kistler's single-axis accelerometer,8316A2D0, is used, and the capacity is ±2g. In order to ensure proper removal of inertial force, the sinusoidal wave excitation of 3 Hz 10 mm experiment without external force was conducted. The force measured by the load cell is plotted with a black line in Figure 2.7 (a), and the force calculated using acceleration and experimental mass is plotted with the red dotted line. The net force calculated from Equation (2.2) is shown in Figure 2.7 (b) and is considered to be a good elimination of inertial force.

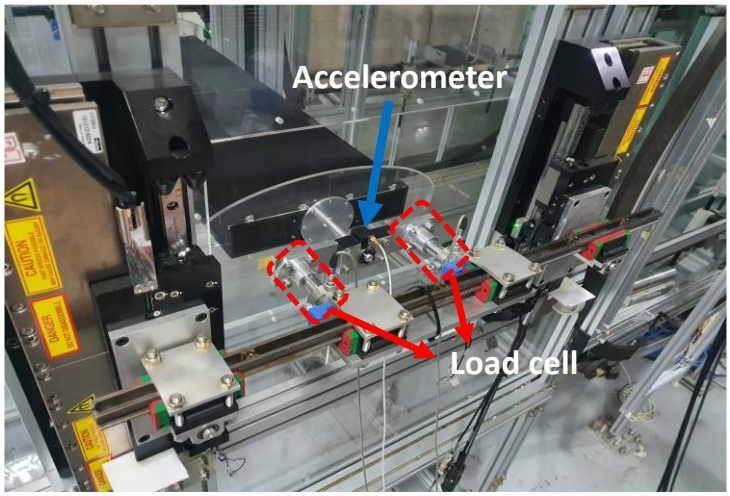

Figure 2.6 Accelerometer in RTAHS system

(a)

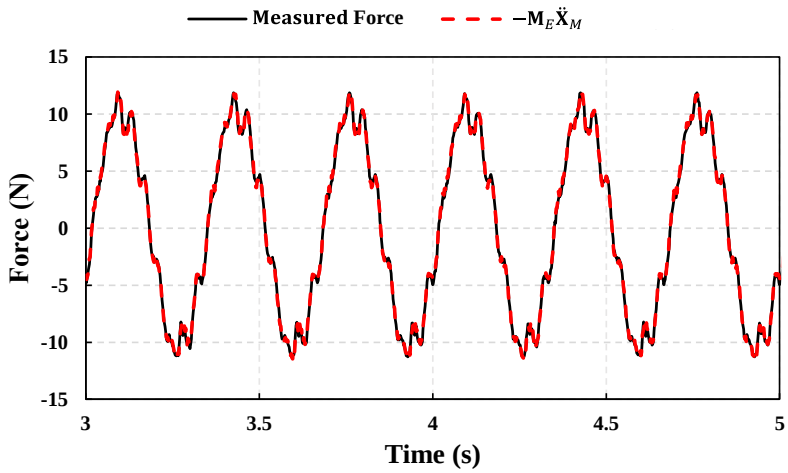

(b)

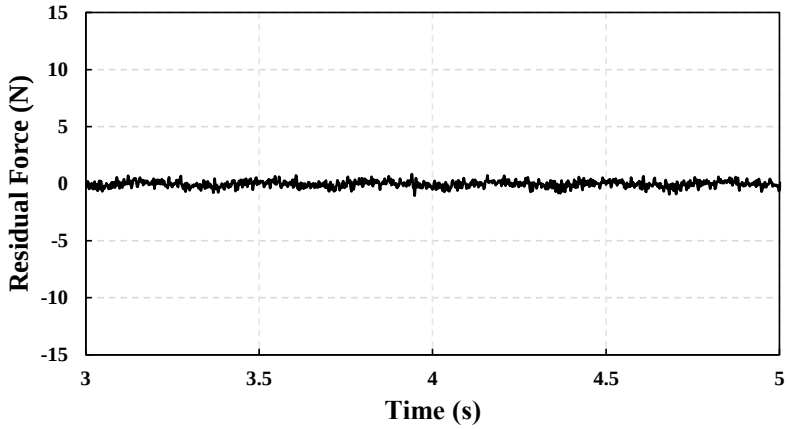

Figure 2.7 Inertial force removal procedure (a) Measured force and inertial force by the accelerometer (b) Net wind-induced force

After calculating the net wind force, the target displacement of the next step is calculated numerically. Numerical methods use the central difference method(CDM), which determines the target displacement of the i+1th step

without using the i+1th step's information. Such methods are called explicit methods.

Taking constant time steps, Δt, the central difference expressions for the velocity and the acceleration at i^{th} step are

$$\dot{\mathbf{X}}_i \cong \frac{1}{2\Delta t}(-\mathbf{X}_{i-1} + \mathbf{X}_{i-1}) \tag{2.3}$$

$$\ddot{\mathbf{X}}_i \cong \frac{1}{2\Delta t^2}(\mathbf{X}_{i-1} - 2\mathbf{X}_i + \mathbf{X}_{i+1}) \tag{2.4}$$

Substituting the above equations into the governing equation, Equation (2.5) is derived.

$$\begin{aligned}\mathbf{X}_{i+1} = \left(\mathbf{M} + \mathbf{C}\frac{\Delta t}{2}\right)^{-1} \Big(\Delta t^2 \mathbf{F}_{w_i} + (2\mathbf{M} - \Delta t^2 \mathbf{K})\mathbf{X}_{M_i} \\ - \left(\mathbf{M} - \mathbf{C}\frac{\Delta t}{2}\right)\mathbf{X}_{M_i-1}\Big)\end{aligned} \tag{2.5}$$

The central difference method has a "blow up" issue that gives meaningless results in numerical round-off if the time step chosen is not short enough. The specific requirement for stability is

$$\frac{\Delta t}{T_n} < \frac{1}{\pi} \tag{2.6}$$

where T_n represents the natural period of vibration of the system. In RTAHS systems, the target frequency area is up to 10 Hz, and the time step is 2 ms, satisfying the condition.

2.2.3 Time-Delay Compensation Scheme

One of the significant factors in RTAHS is control in real-time. The linear motor introduces an inevitable delay when applying command displacements to a structure during a real-time test due to their inherent dynamics. If these time delays are not adequately compensated, they affect the damping ratio and stability, which requires compensation. The time-delay compensation method of Chen et al. (2009,2010; 2012) is applied.

The basic concept of the time-delay compensation method by Chen and Ricles(2009) is shown in Figure 2.8. The command of the target displacement x_{i+1}^{t} is given to the linear motor at the time step t_i, the difference between the time the actual motor reaches that position and the desired time is called a time delay. If the time it took to get to the desired target position is t_d, the motor reaches the target displacement in the time step delayed by $(\alpha - 1)t_d$ at the desired time.

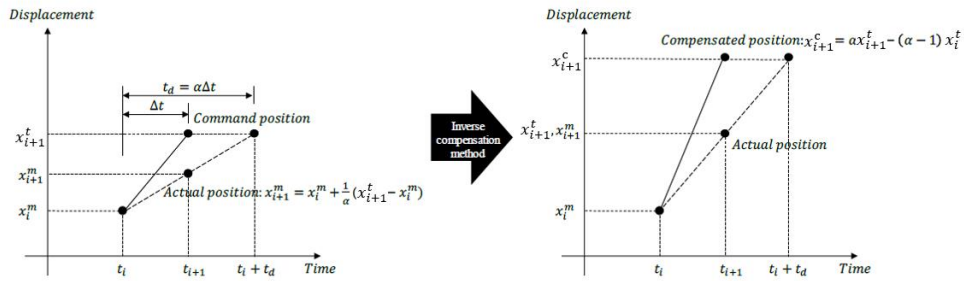

Figure 2.8 Concept of time-delay compensation

Assuming that the transfer function is first-order, the actual position of the linear motor at the time t_{i+1} can be expressed as Equation (2.7).

$$x_{i+1}^m = x_i^m + \frac{1}{\alpha}(x_{i+1}^t - x_i^m) \tag{2.7}$$

Where x_{i+1}^m is the measured displacement at time step t_{i+1}. Applying the discrete z-transform to Equation (2.7) leads to a discrete transfer function $G_d(z)$ is as shown in Equation (2.8).

$$G_d(z) = \frac{X_d^m(z)}{X_d^t(z)} = \frac{z}{\alpha \cdot z - (\alpha - 1)} \tag{2.8}$$

Where $X_d^m(z)$ and $X_d^t(z)$ are the discrete z-transforms of x_{i+1}^m and x_{i+1}^t respectively. Chen proposed to use the inverse of Equation (2.8) for time-delay compensation in real-time testing, whereby the equivalent discrete

transfer function for the resulting inverse compensation method can be written as Equation (2.9).

$$G_c(z) = \frac{X_d^c(z)}{X_d^t(z)} = \frac{\alpha \cdot z - (\alpha - 1)}{z} \tag{2.9}$$

Where $X_d^c(z)$ is the discrete z-transform of x_{i+1}^c, and x_{i+1}^c is the compensated displacements. Applying the inverse discrete z-transform to Equation (2.9), the extrapolation form corresponding to the inverse compensation in the time domain can be expressed as

$$x_{i+1}^c = \alpha x_{i+1}^t - (\alpha - 1) x_i^t \tag{2.10}$$

This method does not consider the effects of time-delay changes due to changes in phase and amplitude and requires a prior understanding of the system's time-delay characteristics. In the real system, the time delay varies depending on the phase and amplitude. Furthermore, misidentifying the time-delay characteristics leads to instability in the system. Thus Chen et al. (2010; 2012) proposed a modified method(Improved Adaptive Inverse Compensation) that includes an adaptive term for changing time-delay($\Delta\alpha$) and an adaptive term for changing amplitude(Δk) as shown in Equation (2.11).

$$G_c(z) = \frac{X_d^c(z)}{X_d^t(z)} = \frac{(k_{est} + \Delta k)[(\alpha_{es} + \Delta\alpha) \cdot z - (\alpha_{es} + \Delta\alpha - 1)]}{z} \quad (2.11)$$

Where α_{es} is the pre-identified time-delay, k_{est} initial estimate of the proportional gain for the motor response, and usually takes the value of 1.0. $\Delta\alpha$ and Δk are evolutionary variable with an initial value of zero, and is determined using the adaptive control law in Equation (2.12) and (2.13).

$$\Delta\alpha(t) = k_p \cdot TI(t) + k_i \cdot \int_0^t TI(\tau)dt \quad (2.12)$$

$$\Delta k(t) = k_p^k \cdot AI(t) + k_i^k \cdot \int_0^t AI(\tau)dt \quad (2.13)$$

Where k_p and k_p^k are the proportional adaptive gains of the adaptive control law, and k_i and k_i^k are the integrative adaptive gains of the adaptive control law. The calculation of the tracking indicator, TI, and the amplitude indicator, AI, are defined in Equation (2.14) and (2.15).

$$TI_{i+1} = 0.5(A_{i+1} - TA_{i+1}) \quad (2.14)$$

$$AI_{i+1} = 0.5(B_{i+1} - TB_{i+1}) \quad (2.15)$$

Where A_{i+1}, TA_{i+1}, B_{i+1} and TB_{i+1} are defined in Equation (2.16)-(2.19).

$$A_{i+1} = A_i + 0.5(d_{i+1}^t + d_i^t)(d_{i+1}^m - d_i^m) \tag{2.16}$$

$$TA_{i+1} = TA_i + 0.5(d_{i+1}^t - d_i^t)(d_{i+1}^m + d_i^m) \tag{2.17}$$

$$B_{i+1} = B_i + 0.5(d_{i+1}^t - d_i^t)(d_{i+1}^t - d_i^t) \tag{2.18}$$

$$B_{i+1} = B_i + 0.5(d_{i+1}^t - d_i^t)(d_{i+1}^t - d_i^t) \tag{2.19}$$

CHAPTER 3

VERIFICATION OF THE RTAHS SYSTEM

The RTAHS system's main parts are real-time control, measuring force, and numerical calculation of the equation of motion. Hardware and software for the RTAHS system have been built, and verification of this system is required before application to wind tunnel test.

First, the compensation method is applied to evaluate the time-delay compensation method. First, the time-delay compensation method is evaluated by conducting a sine sweeping test. The sine signal used in sine sweeping test is made by the calculation of the equation of motion to verify the calculation of the system.

Second, the force-balanced test was conducted to verify that the load cell measures the wind-induced force and compared it with the conventional wind tunnel test.

3.1 Verification of Time-Delay Compensation Method in the RTAHS System

3.1.1 Estimation of Time-Delay RTAHS System

As mentioned in the previous chapter, real-time control requires the application of time-delay compensation methods. The identification of time-delay characteristics of the developed RTAHS system is needed to properly apply the Improved Adaptive Inverse Compensation(Improved AIC) method. Bode plot was used for this purpose.

The Bode plot is a graph of the frequency response of a system. It is usually a combination of a magnitude plot, expressing the frequency response's magnitude, and a phase plot, representing the phase shift.

The random signal with the maximum amplitude of 1 mm and the frequency range of 0.1 Hz to 10 Hz, which is mainly targeted in wind tunnel tests, was used as the target signal for the bode plot. The target displacement and measured displacement are shown in Figure 3.1.

(a)

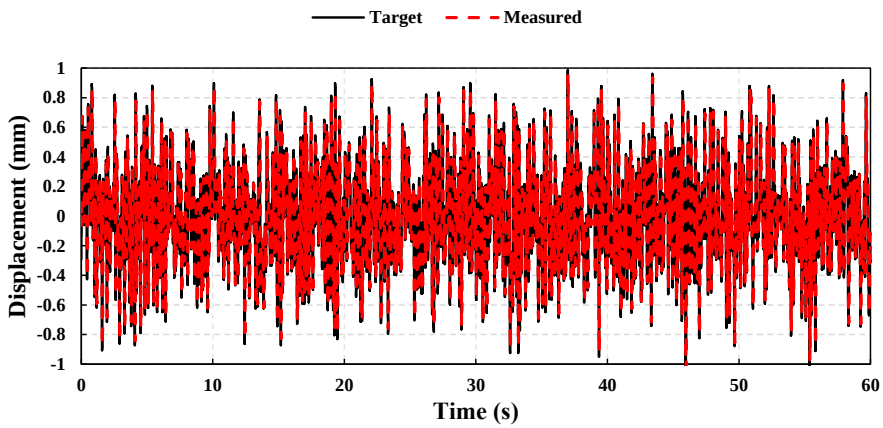

(b)

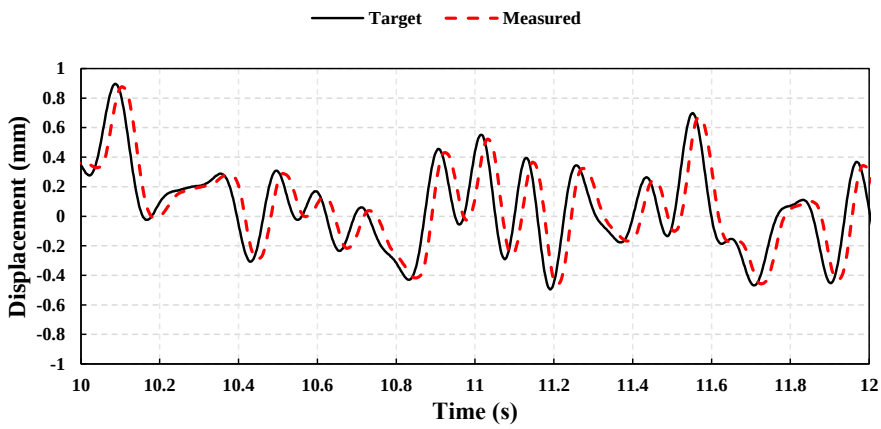

Figure 3.1 Comparison of target and measured displacements using random signal before applying the compensation method
(a) 0~60 sec region (b) 10~12 sec region

System identification algorithm provided by MATLAB (R2020a) was utilized for the bode plot with time-series data, and the result is shown in Figure 3.2.

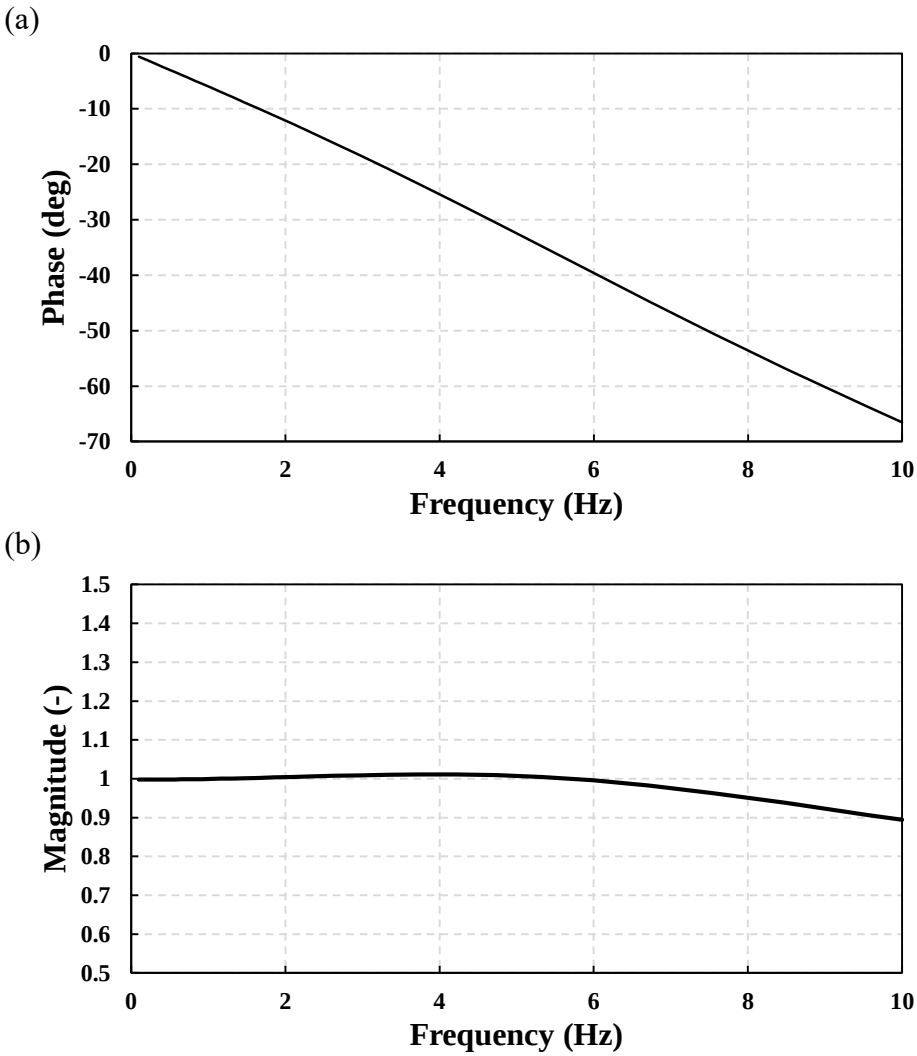

Figure 3.2 Bode plot of RTAHS system (a) Phase shift (b) Magnitude

The magnitude plot shows that the amplitude ratio is almost 1. To estimate the initial constant time delay, frequency and phase are expressed as primary function passing through the origin, and the relationship is shown in Equation (3.1).

$$Phase(deg) = -6.578 \cdot f \tag{3.1}$$

Using this slope, it is calculated that the time delay of the system is approximately 18 ms.

3.1.2 Application of Time-Delay Compensation Method: Sine Sweeping Test

The time-delay characteristic of the RTAHS system was identified, and to check the effect of the Improved AIC method, a sine sweeping test was conducted. This requires the target signal.

To generate the target signal in real-time, a numerical integration loop built in the RTAHS system was used. For this purpose, the target mass is inputted as 60 kg, and the target ratio with 0 % and the frequency of the vibration varies from 1 to 4 Hz, and the corresponding value of K is used. The maximum amplitude of 10 mm and 10 seconds for each frequency. The calculation is made without measuring the force only to verify the numerical integration loop. The sampling rate is 500 Hz, the numerically calculated displacement by Matlab(2020a), and the target displacement calculated in the numerical integration loop is shown in Figure 3.3.

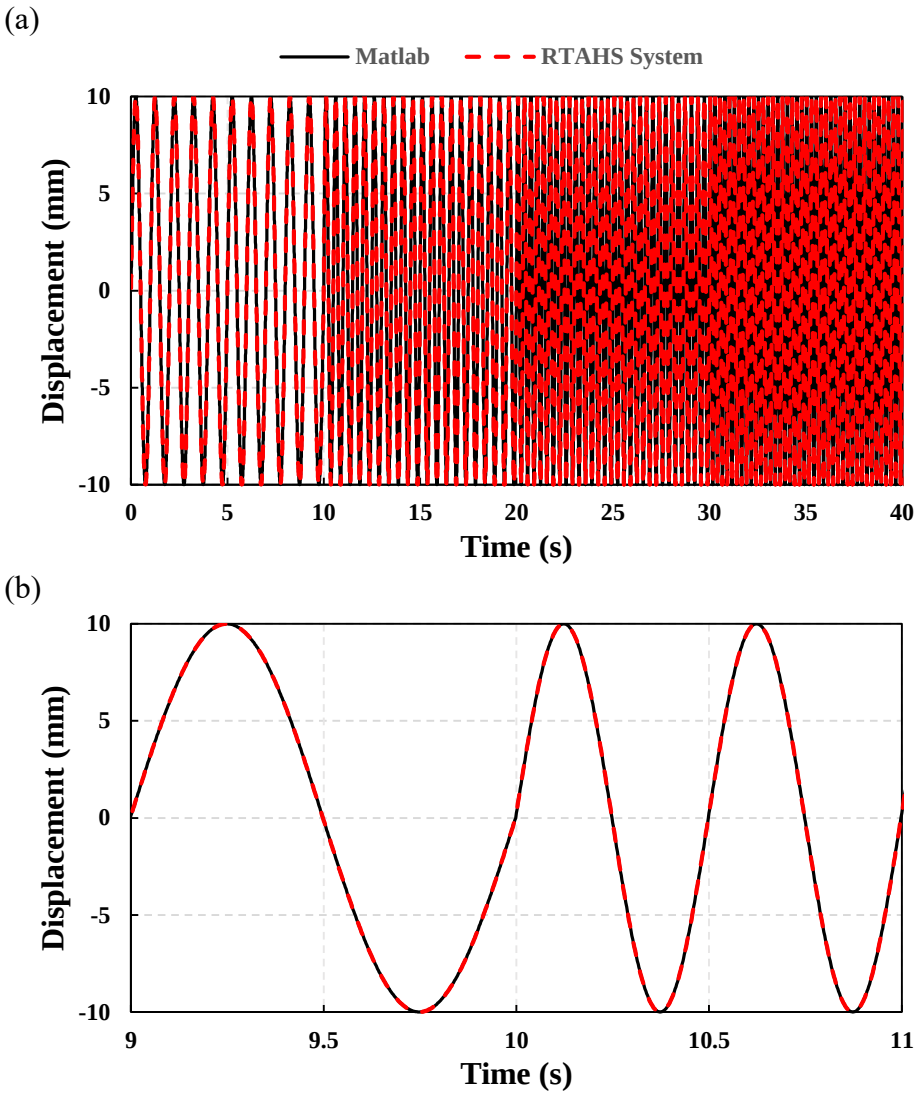

Figure 3.3 Comparison of target signal for sine sweeping test
(a) 0~40 region (b) 9~11 sec region

It was confirmed that there was no difference between the two and that the numerical integration loop was properly calculating the target displacement within the 2 ms. There is no force feedback process in the sine sweeping test

using force measurements, so the target signal is always the same despite target signals are generated in real-time if there is no change in inputted dynamic characteristics.

To check the effect of the Improved AIC method, the measured displacement of two conditions in which the compensation method is not applied and the compensation method is applied is compared with the signal in Figure 3.3, generated in real-time. $\alpha = 9$ is applied according to the system characteristics identified in the previous section and at the suggestion of Chen et al. (2010; 2012), the other parameters for the compensation of $k_{est} = 1.0$, $k_p = 0.4, k_i = 0.04, k_p^k = 2, k_i^k = 0.2$ were applied.

The time-series data of target and measured displacement when compensation is not applied and applied are shown in Figure 3.4 and Figure 3.5, respectively. To check the effect of variable time delay by frequencies, each figure includes zoomed figure at the frequency changing point.

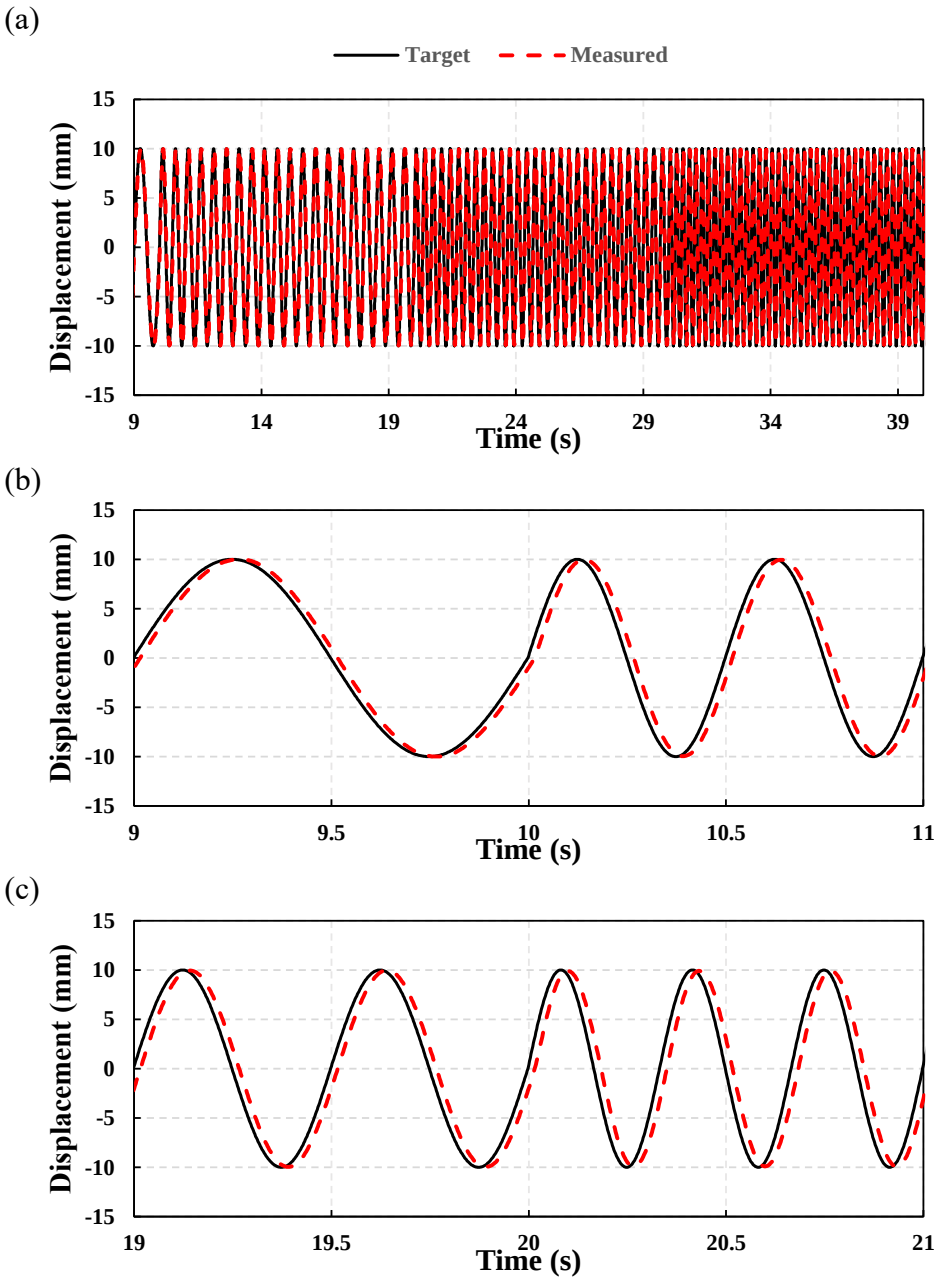

Figure 3.4 Comparison of target and measured displacement of sine sweeping test without delay compensation (a) 0~40 sec region (b) 9~11 sec region (c) 19~21 sec region

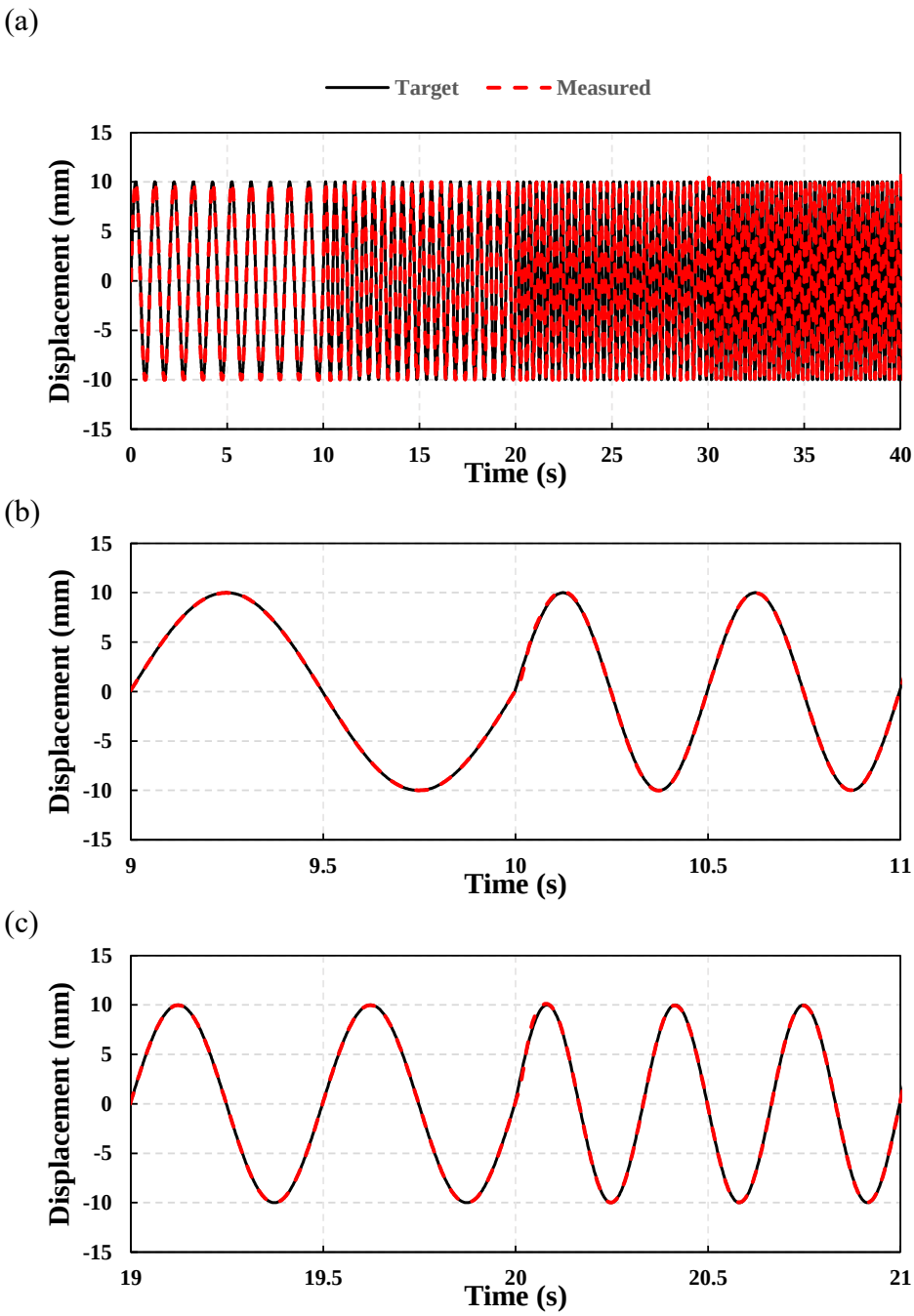

Figure 3.5 Comparison of target and measured displacement of sine sweeping test with delay compensation (a) 0~40 sec region (b) 9~11 sec region (c) 19~21 sec region

As shown in Figure 3.4 and Figure 3.5, the time delay between the target and the measured one is much smaller when applying the compensation method. For a more detailed comparison, the NRMS value in Equation (3.2) is used.

$$\mathrm{NRMS} = \sqrt{\frac{\sum_{i=1}^{N}(x_i^t - x_i^m)^2}{\sum_{k=1}^{N}(x_i^t)^2}} \tag{3.2}$$

Where, x_i^t is a target displacement at the ith step, x_i^m is a measured displacement at the ith step. The lower the NRMS value, the difference between two displacements is small. Evaluated NRMS values are shown in Table 3.1. It can be seen that the NRMS value of the signal applied with the compensation is much smaller.

Table 3.1 Comparison of NRMS value

NRMS (%)	
W/o Compensation	W/ Compensation
31.16	0.86

Figure 3.6 shows the time delay and magnitude for each excitation frequency. Before the compensation method is applied, the time delay is approximately 18 ms, giving the same results as the previously observed system characteristics in random signal excitation. The time delay after applied the

compensation method is within 1 ms. In terms of magnitude, it was also confirmed that it gave better results than before the compensation was applied with an error of less than 1.4 %, and that the compensation method was properly applied.

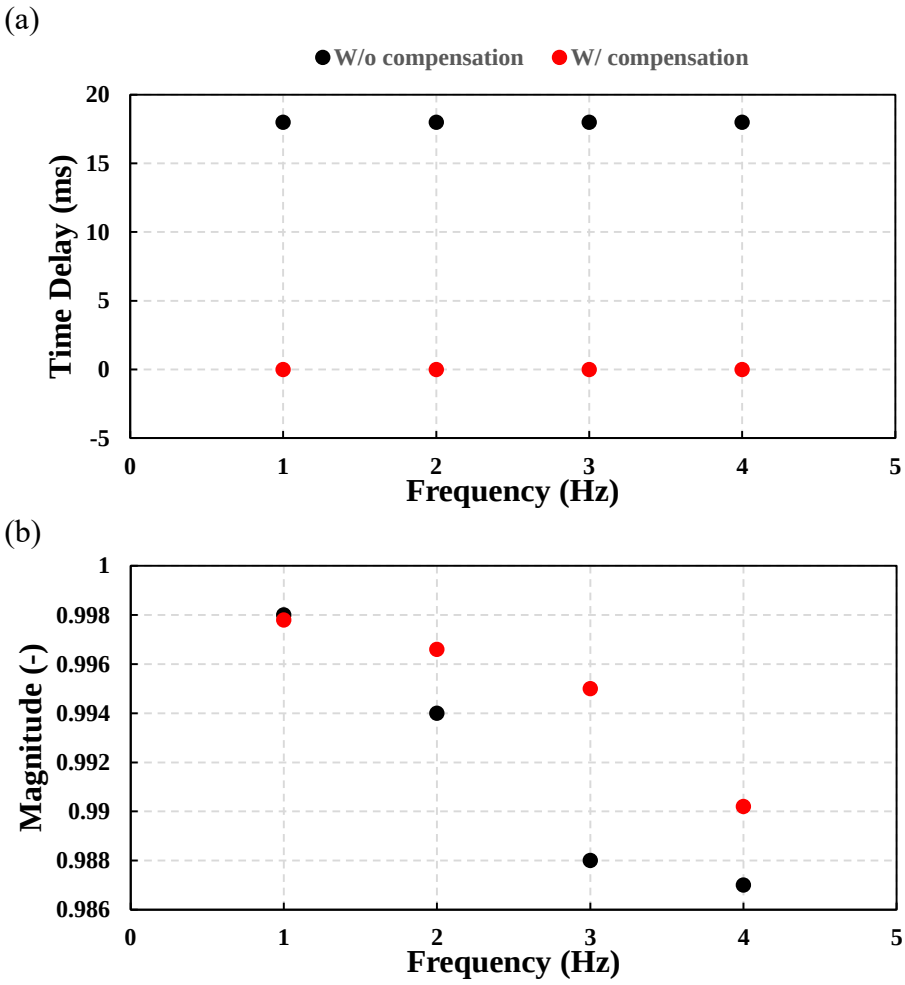

Figure 3.6 Frequency domain comparison of with and without compensation (a) Time delay (b) Magnitude

3.2 Force Balanced Test

3.2.1 Wind Load Measurement System and Test Section

Another essential factor in the RTAHS system is the real-time measurement of wind-induced force. The force balance test was conducted to measure the average wind force actiong on the model. The experiment to measure the variations of aerodynamic coefficients was performed at the wind tunnel at Seoul National University. The wind tunnel is an opened circuit wind tunnel, and the available range of wind speed is from 1 m/s to 23 m/s. The width of the test section is 1.0 m, the height is 1.5 m, and the length is 4.0 m.

Three aerodynamic forces acting on the model were measured using MBA 400 in Figure 2.2. The data collecting time for a single record is 60 seconds at a sampling frequency of 500 Hz, and the averaged value was taken to estimate aerodynamic coefficients. Three aerodynamic coefficients were calculated according to Equations (3.3).

$$C_D = \frac{F_D}{\frac{1}{2}\rho U^2 B} \qquad C_L = \frac{F_L}{\frac{1}{2}\rho U^2 B} \qquad C_M = \frac{F_M}{\frac{1}{2}\rho U^2 B^2} \tag{3.3}$$

In Equation (3.3), C_D, C_L, and C_M are the aerodynamic coefficients for drag force, lift force, lift force, moment force where F_D, F_L, F_M are the corresponding averaged forces and moment acting on the center of gravity of a

section model. ρ is the air density (=1.225 kg/m^3), U is the upcoming wind speed, and B is the width of the deck model. Figure 3.7 shows the sign convention of all the forces acting on a deck model. In the figure, ψ is the wind attack angle that the model experiences. The test section is the bluff body section of B/D = 5, shown in Figure 3.8 where D is the depth of the model.

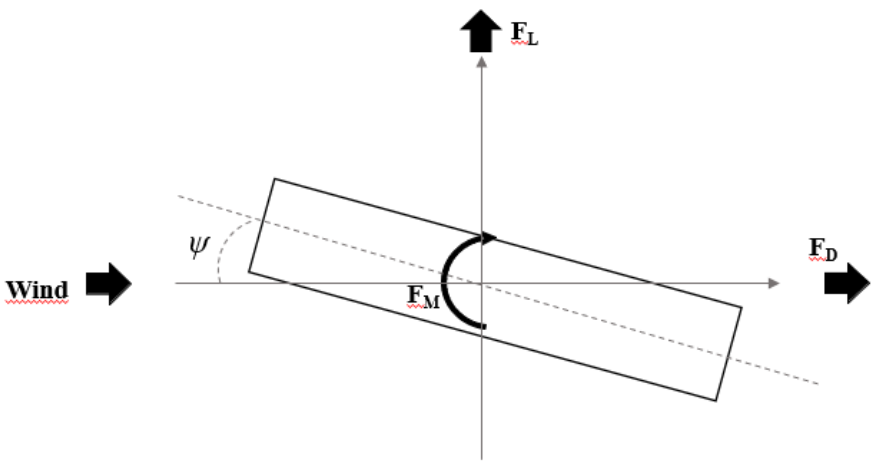

Figure 3.7 Sign convention of aerodynamic forces

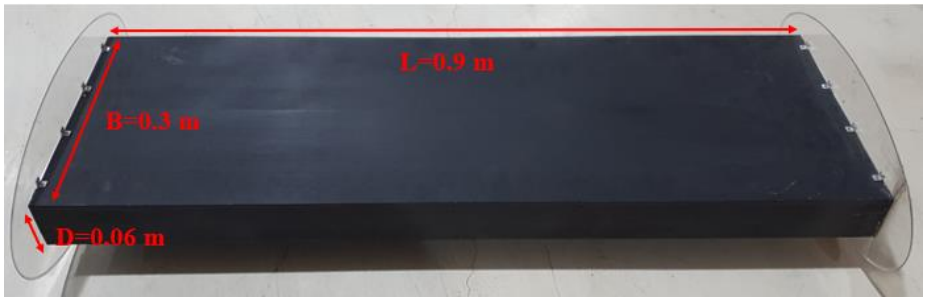

Figure 3.8 Test section model (B/D=5)

3.2.2 Aerodynamic Coefficients under Uniform Wind Condition

The experiments were conducted on the section using the RTAHS system and conventional system to verify the accuracy of measuring the wind-induced force in the RTAHS system,

The wind speed applied in the tests is 10 m/s, and turbulence intensity along the wind direction is maintained at less than 1%. The wind attack angle is varied from – 6 degrees to + 6 degrees in 3 degrees intervals, and the force coefficients by Equation (3.3) at each attack angle is expressed in Figure 3.9, Table 3.2, and Table 3.3 and it can be seen the overall size of the values are similar.

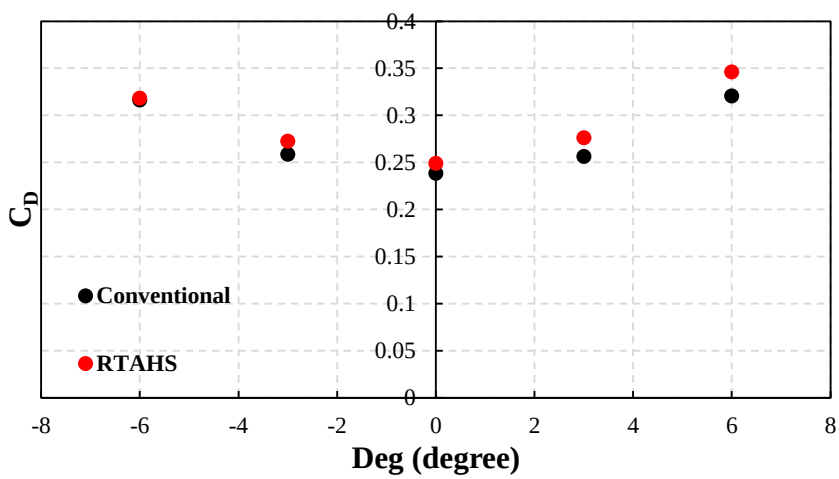

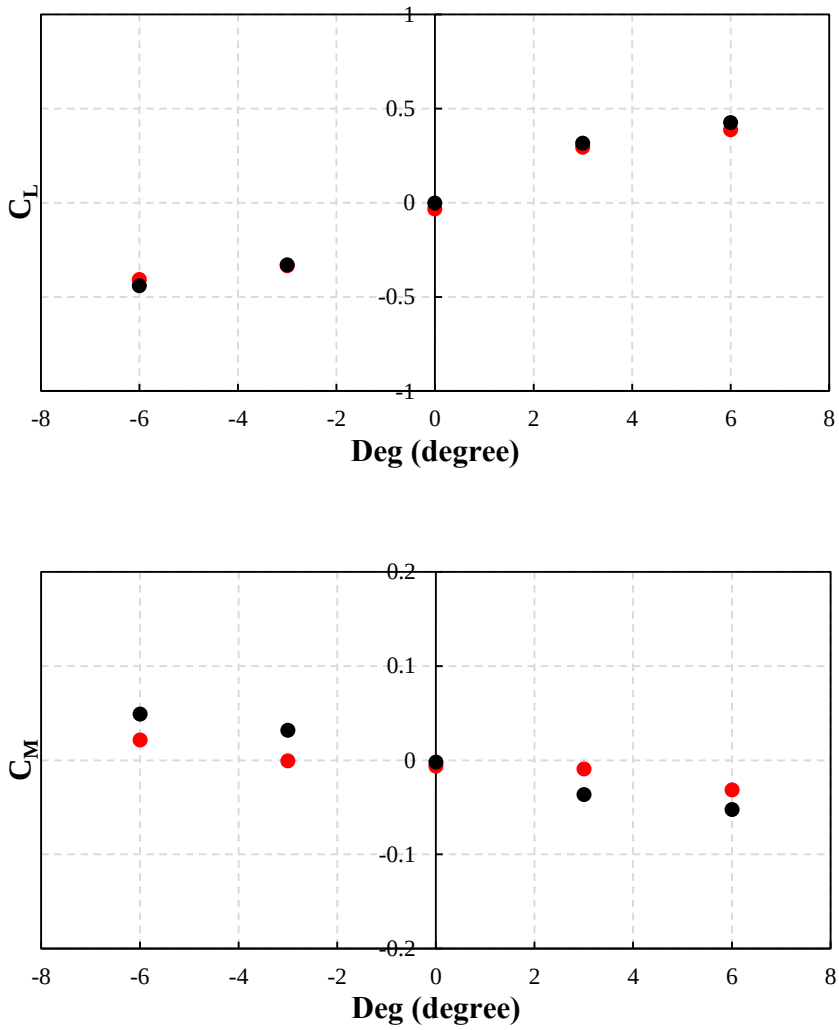

Figure 3.9 Comparison of the measured aerodynamic coefficient

Table 3.2 Measured aerodynamic coefficient by the RTAHS system

Wind Attack Angle (Deg)	C_D	C_L	C_M
-6	0.318357	-0.40858	0.021261
-3	0.272683	-0.3353	-0.00092
0	0.249168	-0.0341	-0.00644
3	0.276278	0.294265	-0.00937
6	0.346219	0.387224	-0.03155

Table 3.3 Measured aerodynamic coefficient by the conventional system

Wind Attack Angle (Deg)	C_D	C_L	C_M
-6	0.314069	-0.44341	0.048959
-3	0.256529	-0.32893	0.031576
0	0.239039	-0.00181	-0.0022
3	0.259385	0.320959	-0.03668
6	0.32225	0.432646	-0.05253

CHAPTER 4

HYBRID TEST FOR VALIDATION OF THE RTAHS SYSTEM

In the previous section, each element of the RTAHS system is verified. Two experiments were conducted to validate the RTAHS system when all elements(numerical integration scheme, force measurment, and inertial force removal process) are operated simultaneously. The model in Figure 3.8 is used for experiments.

First, free vibration experiments were carried out without wind load. There is no wind-induced force, but the inertial force due to vibrations of the model is measured in the load cell. This is eliminated with the acceleration measured through the accelerometer and the mass of the model. The model moves as the target displacement calculated by Equation (2.5) with pre-inputted dynamic properties, measured forces, and acceleration.

Secondly, the aeroelastic wind tunnel test was conducted to measure the bridge model's displacement as the wind speed increases, just like the conventional spring support test. Tests were conducted focusing on verifying that vortex-induced vibration(VIV) due to vortex can be reproduced equally.

4.1 Free Vibration Test

4.1.1 Inputted Dynamic Characteristics and Apparent Dynamic Characteristics

Free vibration tests were conducted without wind load for the validation test of the RTAHS system. Load cells measure the inertial force ($\mathbf{F}_M$) caused by the vibration of the model. In the numerical integration loop installed in the motion controller, inertial forces are removed using simultaneously measured acceleration by the accelerometer($\ddot{\mathbf{X}}_M$) and the mass of the deck model($\mathbf{M}_E$), and the target displacement of the next step is calculated using numerically inputted dynamic characteristics. Furthermore, the Improved AIC method was applied to compensate 18 ms time delay between target displacement and actually measured displacement. When the linear motor receives a command signal and moves, the same process is repeated by utilizing measured displacement, force, and acceleration. Each step is done within 2 ms.

The experiments are carried out in vertical motion with three target masses (M =15, 30, 60 kg), four target damping ratios (ζ_t =0.2, 0.4, 0.6, 0.8 %), and three target frequencies (f_t =3, 4, 5 Hz). The initial displacement was 0.01 mm for 3,4 Hz and 0.005 mm for 5 Hz, and the initial velocity was set to 0 m/s. The data collecting time for a single experiment is 60 seconds. The experimental mass of the model is 2.974 kg. Three replicates were conducted

for each condition, and a total of 108 experiments were conducted. The overall experimental setup is shown in Figure 4.1.

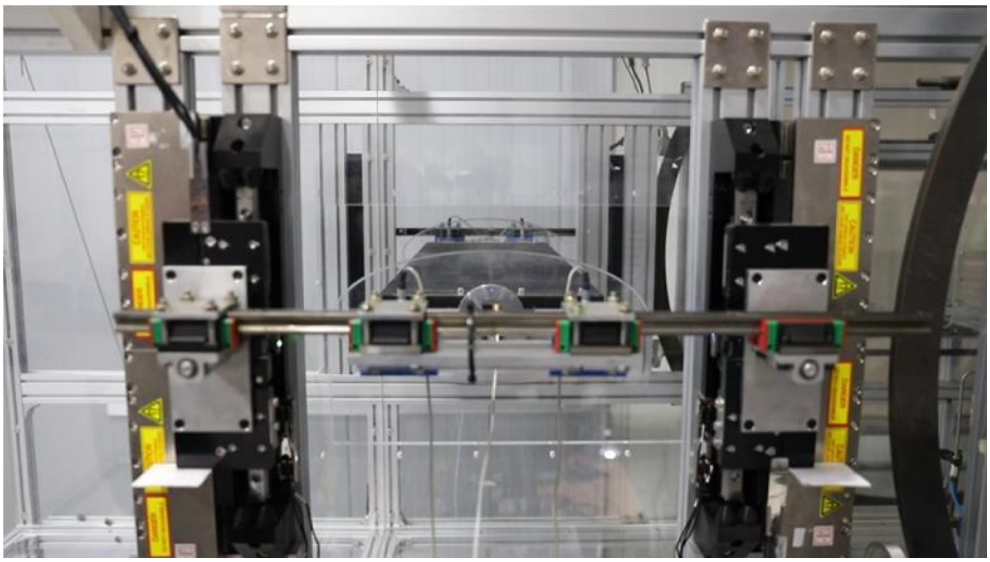

Figure 4.1 Experimental setup for free vibration test

The results of the experiment are shown in Table 4.1 and Figure 4.2. The apparent dynamic characteristics are compared to the target values, using a mean value of three times. The apparent frequency of the vibration was achieved through the FFT of the measured time-series data, and the apparent damping ratio was calculated by the logarithmic decrement using measured displacement data from 90% to 20% of the initial displacement.

Table 4.1 Free vibration test results

		M (kg)					
		60		30		15	
f_t (Hz)	ζ_t (%)	f_m (Hz)	ζ_m (%)	f_m (Hz)	ζ_m (%)	f_m (Hz)	ζ_m (%)
3	0.2	3.00	0.25	3.00	0.28	3.01	0.36
	0.4	3.00	0.45	3.00	0.49	3.01	0.56
	0.6	3.00	0.65	3.00	0.69	3.01	0.80
	0.8	3.00	0.85	3.00	0.89	3.01	0.96
4	0.2	4.00	0.21	4.00	0.20	4.01	0.21
	0.4	4.00	0.41	4.00	0.41	4.01	0.40
	0.6	4.00	0.61	4.00	0.61	4.01	0.61
	0.8	4.00	0.81	4.00	0.81	4.00	0.81
5	0.2	5.00	0.22	5.00	0.24	5.00	0.29
	0.4	5.00	0.42	5.00	0.44	5.00	0.49
	0.6	5.00	0.63	5.00	0.65	5.00	0.69
	0.8	5.00	0.84	5.00	0.86	5.00	0.88

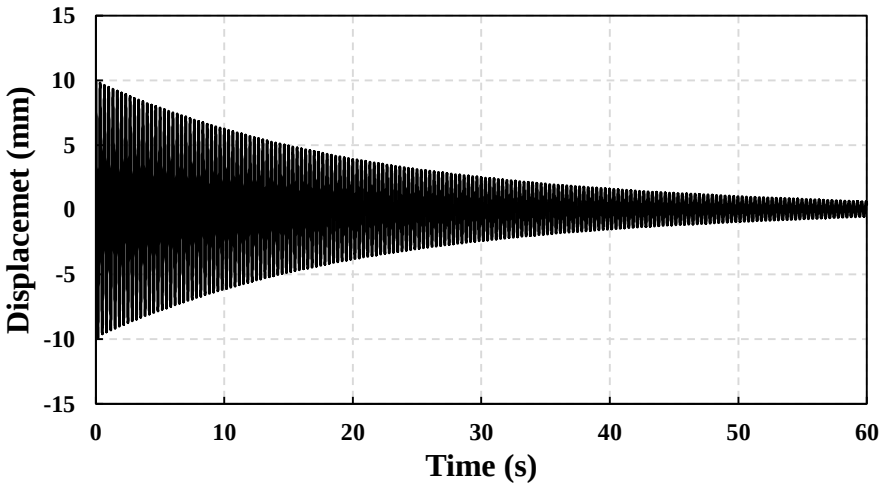

Figure 4.2 Time series data of free vibration test
(M =60 kg, ζ_t =0.2 %, f_t =3 Hz)

As can be seen from Table 4.1, it can be seen that the system implements the target value well for the frequency of vibration. Figure 4.2 shows that the measured displacement has the shape of free vibration. Still, in the case of the apparent damping ratio, it tends to be measured somewhat higher than the target value, and the additional damping ratio is shown in Figure 4.3 of the 3 Hz experiment.

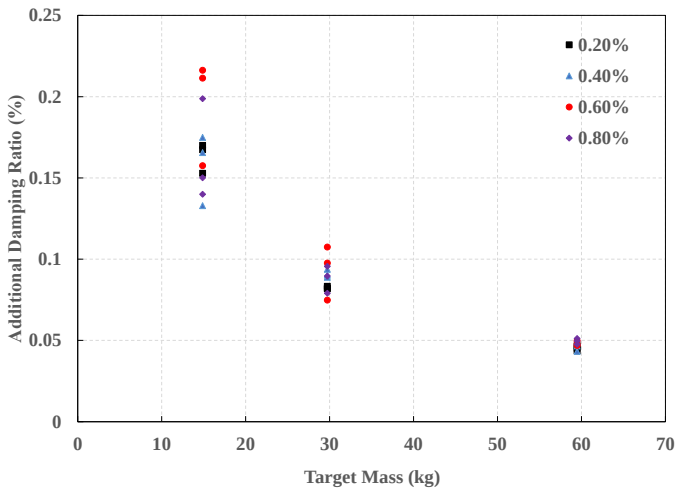

Figure 4.3 Additional damping ratio of 3 Hz test result

4.1.2 Apparent Daping Ratio and the Time Dealy

An understanding of this additional damping ratio is required. The previous study (Moni et al., 2020) has observed this phenomenon and has confirmed that it is caused by a time delay between the target signal and the measured force by the load cell.

Reflecting the current system's characteristics, the time delay between target displacement and measured force, acceleration was considered. Consider an RTAHS system of SDOF harmonic motion, with an angular frequency of ω_t and amplitude of A_0 as in Equation (4.1).

$$x_t(t) = A_0 \sin(\omega_t) \tag{4.1}$$

The Measured acceleration($\ddot{x}_M$) and force(f_M) with a time delay of t_d^{load} and t_d^{acc} is shown in Equation (4.2) and Equation (4.3).

$$\ddot{x}_M(t) = -\mathrm{A}_0 \omega_t^2 \sin\left(\omega_t (t - t_d^{acc})\right) \tag{4.2}$$

$$f_M(t) = A_0 \omega_t^2 M_E \sin\left(\omega_t \left(t - t_d^{load}\right)\right) \tag{4.3}$$

Where, t_d^{acc} is a time delay between target displacement and measured acceleration, t_d^{load} is a time delay between target displacement and measured force.

These time delays make the residual force in Equation (2.2) though there is no external force. For each cycle, the residual force inputs energy to the system, as shown in Equation (4.4).

$$\begin{aligned} E_t &= \int_0^T -(f_m + M_E \ddot{x}_m) \frac{dx_t}{dt} dt \\ &= \pi A_0^2 \omega_t^2 M_E \left\{\sin\left(\omega_t t_d^{load}\right) - \sin(\omega_t t_d^{acc})\right\} \end{aligned} \tag{4.4}$$

The energy dissipated by viscous damping in each cycle, E_D, can be written as Equation (4.6).

$$E_D = \int_0^T f_D(t)dx = \int_0^T c_{eq}\left(\frac{dx_t}{dt}\right)^2 dt = \pi A_0^2 \omega_t c_{eq} \tag{4.5}$$

Using this relationship that $E_t = E_D$, the equivalent viscous damping can be expressed as Equation (4.6),(4.6) and the corresponding equivalent damping ratio is shown in Equation (4.7).

$$c_{eq} = \omega_T M_E \left\{\sin\left(\omega_t t_d^{load}\right) - \sin(\omega_t t_d^{acc})\right\} \tag{4.6}$$

$$\zeta_{eq} = \frac{c_{eq}}{2\sqrt{MK}} = \frac{c_{eq}}{2\omega_t M} = \frac{1}{2}\left\{\sin\left(\omega_t t_d^{load}\right) - \sin(\omega_t t_d^{acc})\right\}\frac{M_E}{M} \tag{4.7}$$

The additional damping ratio is calculated with Equation (4.7) and actual delay times of load cell and accelerometer from the free vibration test result. And the apparent additional damping ratio is shown in Figure 4.4. The apparent additional damping ratio and the calculated additional damping ratio have a linear relationship. Since it is impossible to make these time delays completely zero, to obtain the desired target damping ratio, a preliminary test for identifying the characteristics of the system are needed

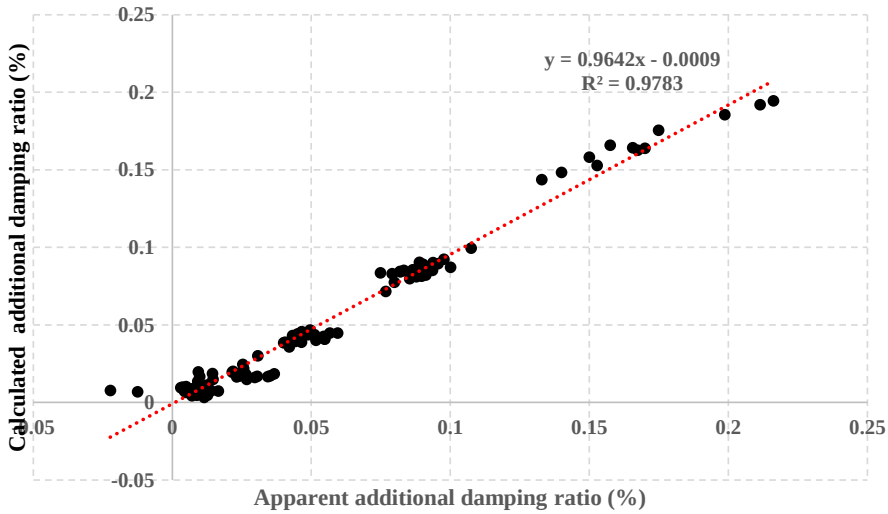

Figure 4.4 Apparent and calculated additional damping ratio

4.2 Aeroelastic Wind Tunnel Test

4.2.1 Vortex-Induced Vibration

When the flowing wind meets a blunt body flow, separation will occur on the body's surface, causing vortices to be shed alternately on either side of the structure. The shedding frequency properties are characteristic of the cross-section of the bridge, and the Strouhal number(*St*), which is used to describe the characteristic of the vortex, is shown in Equation (4.8).

$$St = \frac{f_s D}{U} \tag{4.8}$$

Where f_s is the shedding frequency, D is the dimension of the model, and U is mean wind speed.

As can be seen in Equation (4.8), vortex shedding frequency increases as the wind speed increases. When the vortex shedding frequency gets close to the bridge's natural frequency, lock-in occurs where the vortex shedding frequency does not increase even though wind speed increases, as shown in Figure 4.5, and the bridge resonates with limited amplitude. This phenomenon is called vortex-induced vibration (VIV), which can be seen in many long-span bridges and affects serviceability and fatigue.

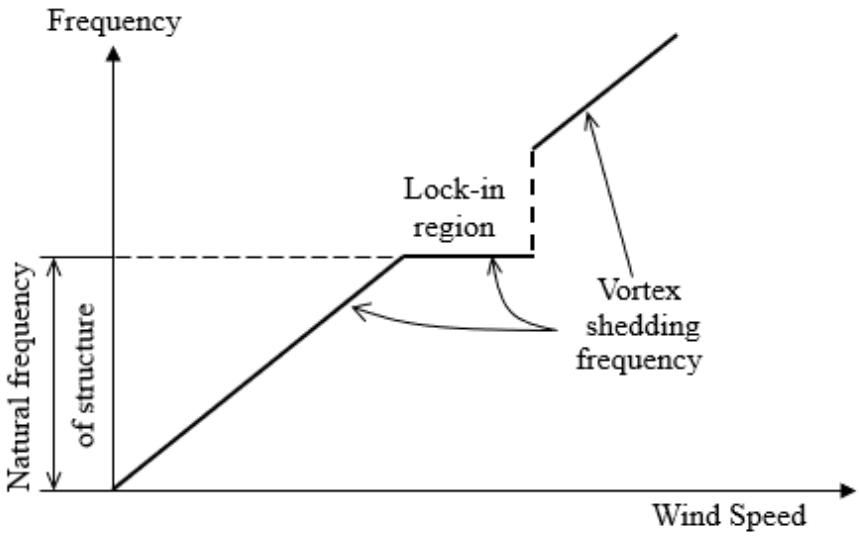

Figure 4.5 Lock-in phenomenon

4.2.2 Wind Tunnel Test

Wind tunnel tests are conducted to verify the bridge's response under wind load, as mentioned in the previous section. The wind tunnel test using the conventional system and the RTAHS system was carried out using a cross-section model of Figure 3.8.

The tests' target frequency is 3 Hz in the vertical, and the target mass is 15 kg. The damping ratio affects the response of the section model. To compare the result, a total of 3 cases of tests were conducted 1 case with conventional and 2 cases with RTAHS system.

For all cases, the free vibration test for identifying the damping ratio is conducted before the main test, and each vibration response is shown in Figure 4.6. The damping ratio was calculated by the logarithmic decrement using measured displacement data from 90% to 20% of the initial displacement. And Table 4.2 shows the experimental setup for the wind tunnel test. For the comparison, the Scruton number (Sc), the important parameter for vortex-induced vibration expressed in Equation (4.9), is applied.

$$Sc = \frac{2\pi\zeta}{\rho B^2} \tag{4.9}$$

(a)

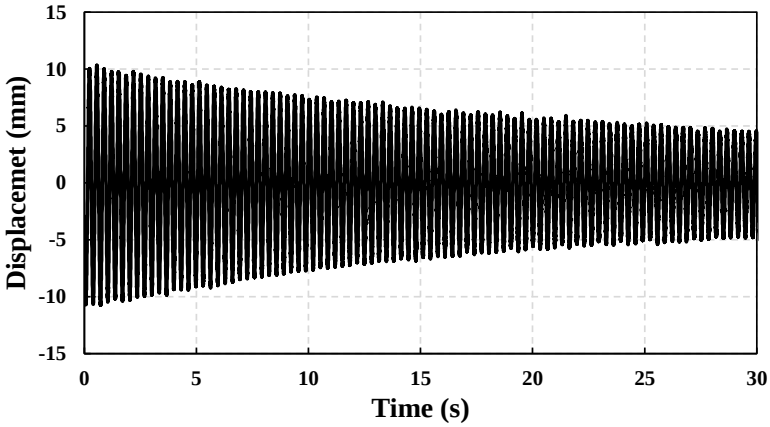

(b)

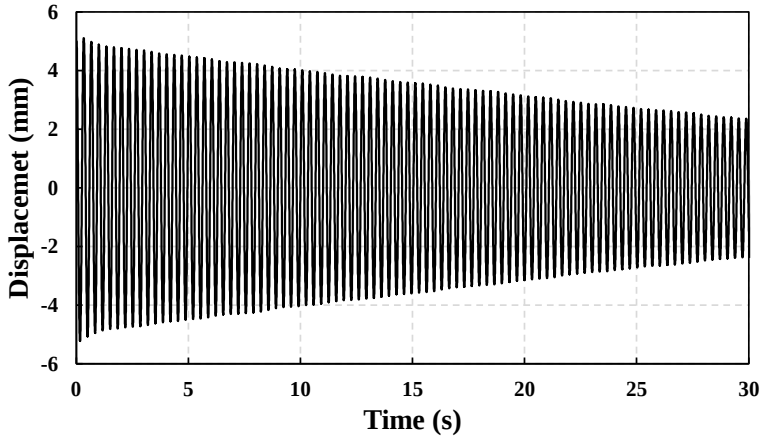

(c)

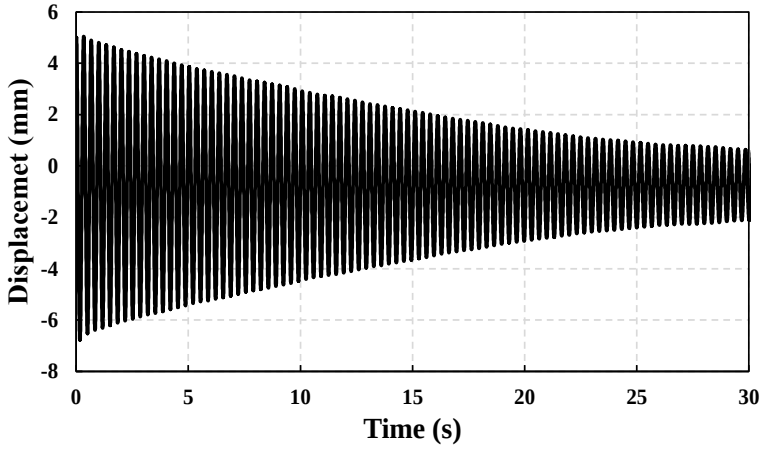

Figure 4.6 Time-series results of free vibration test
(a) Conventional system(Sc=68)
(b) RTAHS system(Sc=128) (c) RTAHS system(Sc=214)

Table 4.2 Test setup parameters

	Conventional system(Sc=68)	RTAHS system(Sc=128)	RTAHS system(Sc=214)
Target mass (kg)	15	15	15
Target frequency (Hz)	3	3	3
Target damping ratio (%)	1.2	2.25	3.75

After the experimental setup, the wind tunnel tests were conducted by increasing the wind speed to 6m/s. The VA curve was utilized to compare the results, showing the vibration's maximum amplitude compared to wind speed. In all three cases, VIV has been observed at wind speed 1.5 m/s to 2.1 m/s. The maximum amplitude of VIV is known to be inversely proportional to the power of Scruton number, and based on this, and the RTAHS system is considered applicable to the wind tunnel.

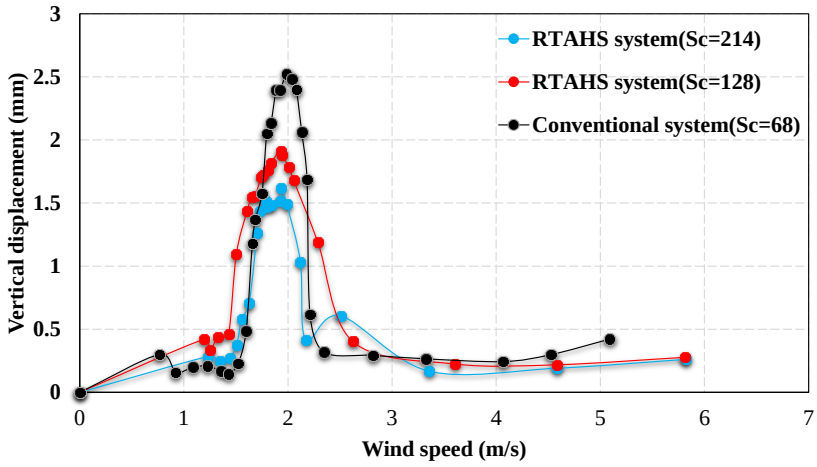

Figure 4.7 Wind tunnel test results(VA curve)

CHAPTER 5

CONCLUSIONS AND RECOMMENDATIONS FOR FURTHER STUDY

The new concept of wind tunnel test by using real-time hybrid simulation methodology was developed in this study to advance conventional wind tunnel test. In this paper, the proposed RTAHS system performs wind tunnel tests in two parts, virtual and physical. In the physical part, wind-induced forces are measured through real testing, and in the virtual system, displacement of bridge models is calculated with inputted dynamic and measured forces. Through this, it can have significant advantages compared to the conventional wind tunnel test. First, by applying the RTAHS system to the wind tunnel test, the wind-induced force is measured directly through actual test without any assumptions. Second, dynamic characteristics are accurately and efficiently simulated compared to the conventional one.

For the development of the proposed RTAHS system, hardware and software systems were built. The hardware part consists of a load cell for measuring wind force, an accelerometer for measuring acceleration for inertial force removal, a motion controller for control systems, and the linear motor for giving deck motion.

The control system, the software for control of the linear motor, consists of PI control for precision control, time-delay compensation loop for time delay

due to the linear motor's characteristics, and a numerical integration loop to measure the net wind-induced force and calculate the next step's displacement.

The software system was verified through a series of experiments: (1) Time-delay compensation test, (2) Force balanced test. It was confirmed that the time delay compensation method proposed by Chen et al.(2012) appropriately compensates for the time delay of 18 ms. The numerical integration loop is also properly performed within 2 ms. It was confirmed that the proposed RTAHS system is applicable to the wind tunnel test through validation test.

Many potential benefits of RTAHS systems are proposed. First, It reduces the time for setup dynamic characteristics for experiments. Secondly, the new concept can be applied to simulate wind tunnel tests' response under multi-mode conditions. Third, the new system is valid for evaluating the response of multi-mode buffetting responses.

To improve the performance of the proposed RTAHS system, the following subjects are recommended for future research. First, it is recommended to modify the algorithm for motor control for more precise control. The motor's control method has a significant change in response, which has a significant impact on the experimental results. Second, improvements in time-delay compensation methods are needed. The residual time delay after compensation expressed by the time delay of the accelerometer and load cell affects the system response. Furthermore, for consideration of multi-mode response, compensation method for multi-mode are needed.

REFERENCE

Chae, Y., et al. (2013). Adaptive time series compensator for delay compensation of servo-hydraulic actuator systems for real-time hybrid simulation. Earthquake Engineering & Structural Dynamics, 42(11), 1697-1715.

Chen, C., & Ricles, J. M. (2009). Analysis of actuator delay compensation methods for real-time testing. Engineering Structures, 31(11), 2643-2655.

Chen, C., & Ricles, J. M. (2010). Tracking Error-Based Servohydraulic Actuator Adaptive Compensation for Real-Time Hybrid Simulation. Journal of Structural Engineering-ASCE, 136(4), 432-440.

Chen, C., et al. (2012). Improved Adaptive Inverse Compensation Technique for Real-Time Hybrid Simulation. Journal of Engineering Mechanics-ASCE, 138(12), 1432-1446.

Kanda, M., et al. (2006). Numerical integration scheme for hybrid vibration technique–explicit scheme equivalent to unconditionally stable. Journal of Wind Engineering and Industrial Aerodynamics, 31,1.

Kato, Y., & Kanda, M. (2014). Development of a modified hybrid aerodynamic vibration technique for simulating aerodynamic vibration of structures in a wind tunnel. Journal of Wind Engineering and Industrial Aerodynamics, 135, 10-21.

Mercan, O., & Ricles, J. M. (2007). Stability and accuracy analysis of outer-loop dynamics in real-time pseudodynamic testing of SDOF systems. Earthquake Engineering & Structural Dynamics, 36(11), 1523-1543.

Mosqueda, G., et al. (2007). Real-time error monitoring for hybrid simulation. Part II: Structural response modification due to errors. Journal of Structural Engineering-ASCE, 133(8), 1109-1117.

Scanlan, R. (1978a). The action of flexible bridges under wind, I: flutter theory. Journal of Sound and Vibration, 60(2), 187-199.

Scanlan, R. (1978b). The action of flexible bridges under wind, II: Buffeting theory. Journal of Sound and Vibration, 60(2), 201-211.

Scanlan, R. H., & Tomo, J. (1971). Air foil and bridge deck flutter derivatives. Journal of Soil Mechanics & Foundations Div.

Strømmen, E. (2010). Theory of bridge aerodynamics: Springer Science & Business Media.

Wu, T., & Song, W. (2019). Real-time aerodynamics hybrid simulation: Wind-induced effects on a reduced-scale building equipped with fullscale dampers. Journal of Wind Engineering and Industrial Aerodynamics, 190, 1-9.

Chen C. et al. (2009) Real-time hybrid testing using the unconditionally stable explicit CR integration algorithm. Earthq Eng Struct Dyn 2009, 38(1), 23-44.

Mercan O. (2007) Analytical and experimental studies on large scale, real-time pseudodynamic testing. Ph.D. dissertation. Department of Civil and Environmental Engineering, Lehigh University.

Ogata K. (1995) Discrete-time control systems. 2nd ed. Prentice-Hall.

Kanda, M., et al. (2003). A new approach for simulating aerodynamic vibrations of structures in a wind tunnel-Development of an experimental system by means of hybrid vibration technique. Journal of Wind Engineering and Industrial Aerodynamics, 91 (11), 1419–1440.

Kato, Y., and M. Kanda. (2014). Development of a modified hybrid aerodynamic vibration technique for simulating aerodynamic vibration of structures in a wind tunnel. Journal of Wind Engineering and Industrial Aerodynamics. 135 (Dec), 10–21.

Stefanaki, A. (2017). A simple strategy for dynamic substructuring and its application to soil-foundation-structure interaction. Ph.D. dissertation, Department of Civil, Structural and Environmental Engineering, State Univerity of New York at Buffalo.

Stefanaki, A., and M. V. Sivaselvan. (2018). A simple strategy for dynamic substructuring. I: Concept and development, Earthquake Engineering & Structural Dynamics, 47 (9), 1801–1822.

Stefanaki, A., M. V. Sivaselvan, S. Weinreber, and M. Pitman (2018). A simple strategy for dynamic substructuring. II: Experimental evaluation. Earthquake Engineering & Structural Dynamics, 47 (9), 1823–1843.

Yalla, S. K., and A. Kareem (2007). Dynamic load simulator: Actuation strategies and applications. Journal of Engineering Mechanics, 133 (8), 855–863.

Yalla, S. K. et al. (2001). Dynamic load simulator: Development of a prototype. Journal of Engineering Mechanics, 127 (12), 1310–1315.

Y. Hwang. (2019). Hybrid Simulation System for the Aeroelastic Phenomena of the Bridge Deck. Ph.D. dissertation, Department of Civil & Environmental Engineering, Seoul National Univerity.

Moni, M., et al. (2020). Real-Time Aeroelastic Hybrid Simulation of a Base-Pivoting Building Model in a Wind Tunnel. Frontiers in Built Environment, 6, 157.

국 문 초 록

심재홍
건설환경공학부
서울대학교 대학원

이 연구에서는 교량의 풍동실험을 위한 새로운 기법을 제시하며, 이를 위한 장비를 개발 및 구축하고 구축된 장비를 활용하여 실제 풍동실험에의 적용가능성에 대한 검토를 목표로 한다. 제안된 새로운 풍동실험 방법은 실시간 하이브리드 기법을 적용하여 풍동실험을 실험적, 수치적 시스템으로 나누어 둘 간의 상호작용을 통하여 수행된다.

실시간 공탄성 하이브리드 시뮬레이션 시스템은 수치적으로 구현하기 어려운 바람에 의한 힘을 실험을 통하여 측정하고 수치적으로 교량 데크의 변위를 실시간으로 계산하는 방식을 사용한다. 이로 기존 풍동실험에서는 측정하기 어려웠던 바람에 의한 힘을 정확히 측정하며, 시스템의 동적 특성은 수치적으로 보다 쉽고 정확히 구현할 수 있다.

실시간 공탄성 하이브리드 시뮬레이션 시스템은 네 개의 리니어 모터와 이를 제어하기 위한 컨트롤러, 로드셀, 가속도계의 하드웨어적인 부분과 운동방정식 계산을 위한 수치 적분 프로그램, 리니어 모터의 정밀한 제어를 시간지연 보상 프로그램, PI 제어 프로그램의 소프트웨어적인 부분으로 이루어진다.

실제 구성한 실시간 공탄성 하이브리드 시뮬레이션 시스템 소프트웨어 각 부분의 검증을 수행하였다. 실험체의 질량 인한 관성력을 제거하며 운동 방정식의 실시간 계산 및 Improved AIC 방법을 통하여 시스템의 총 지연시간 18 ms 의 보정이 적절히 수행됨을 확인하였다.

측정된 힘의 되먹임 과정을 포함하는 자유 진동 실험 및 풍동 내에서의 교량데크의 와류진동을 관측하기 위한 진동실험을 통하여 실제 풍동실험 적용가능성에 대해 확인하였다. 시스템의 겉보기 감쇠비가 다소 차이가 있음을 확인하였으며, 이는 시간지연보상 후의 잔여 시간지연 효과로 인함인 것으로 파악되었다. B/D=5 직사각형 단면의 고안한 장비와 기존 장비를 활용한 비교실험을 통하여 동일 풍속대에서 와류진동을 관측하였으며, 변위 결과 또한 합리적임을 확인하였다. 따라서, 개발한 실시간 공탄성 하이브리드 실험 장비가 확인한 범위 내에서 2 차원 풍동 실험을 잘 모사할 수 있음을 확인하였다.

주요어: 풍동 실험; 실시간 공탄성 하이브리드 시뮬레이션; 시간지연 보상; 교량 데크; 리니어 모터;

Student Number: 2019-26624